Systematic Modeling of Rotor Dynamics for Small Unmanned Aerial Vehicles

Limin Wu*, Yijie Ke and Ben M. Chen
Unmanned Systems Research Group
Department of Electrical and Computer Engineering, Faculty of Engineering
National University of Singapore, 21 Lower Kent Ridge Rd, Singapore 119077

ABSTRACT

This paper proposes a systematic modeling approach of rotor dynamics for small unmanned aerial vehicles (UAVs) based on system identification and first principle based methods. Both static state response analysis and frequency-domain identifications are conducted for rotor, and CIFER software is mainly utilized for frequency-domain analysis. Moreover, a novel semi-empirical model integrating rotor and electrical speed controller is presented and verified. The demonstrated results and model are promising in UAV dynamics and control applications.

1 INTRODUCTION

Rotor dynamics plays a crucial role in understanding flight dynamics for small UAVs with rotor configuration, and the challenges include complex propeller aerodynamics and system hardware response. In current UAV development, the rotor dynamics is usually simplified by utilizing low frequency response information only, such as static thrust and torque. To further improve flight maneuverability, dynamics of the rotor system has to be investigated.

Typically, modeling methods for such system include system identification and first-principle modeling method [1]. Both methods are attempted and realized in our work. On the one hand, system identification can extract the information of system response around a certain trim condition, such as static state and frequency-domain response. The accuracy of this method depends heavily on experiment setup and data processing techniques. In our work, the CIFER software is mainly utilized for frequency response analysis, which can provide a reliable estimation on dynamics response and has been commonly used in flight dynamics identification [3, 4]. On the other hand, first-principle modeling relies on a deep understanding of underlying physics. As the rotor subsystem in UAVs usually consists of motor, propeller and electronic speed controller (ESC), modeling of such integrated subsystem is a challenge, which is also commonly overlooked in the literature to our best knowledge. Thus we propose a semi-empirical method based on experiment data, in order to approximate the subsystem dynamics for flight dynamics and control applications.

The paper is organized as follows: Section 2 presents the experiment setup. Section 3 illustrates the system identification method for rotor response, including both static state analysis and frequency domain analysis. Responses of thrust force, torque and propeller angular speed are recorded and investigated. Section 4 presents a novel semi-empirical method integrating brushless DC motor, propeller and ESC. Conclusions are summarized in section 5.

2 EXPERIMENTS AND CONDITION

The experiment aims to capture dynamics of rotor system under desired condition. Setup of our work is shown in schematics in Figure 1 and 2.

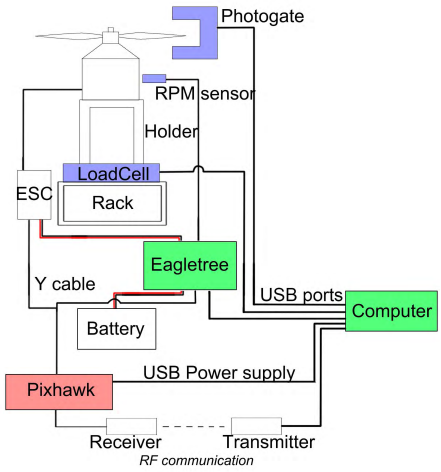

Figure 1: Schematic of rotor test hardware setup

Equipments are listed below in Table 1. The input of rotor system is normalized throttle from 0.0 to 1.0. It is generated by Pixhawk at fixed data rate of 150Hz. Outputs of system are thrust and torque as well as angular speed of rotor. Loadcell can record force and torque in six degree of freedom with fixed logging rate at 1000Hz. Angular speed in RPM can be measured by Eagletree and Photogate devices. Eagletree has a low recording rate of 10Hz and Photogate can record at extremely high frequency which is able to capture every single

*Corresponding author.
Email: a0112849@u.nus.edu

Figure 2: Rotor test setup

Name	Description
APC 11X5.5P Propeller	rotor propeller
Scorpion 3026 motor	brushless DC motor
Scorpion Commander 90A	ESC
4-cells LiPo battery	power supply
optical RPM sensor	angular speed measuring device
Photogate	angular speed measuring device
ATI load cell	6 DOF force and torque logging
Pixhawk	PWM throttle input generator
EagleTree elogger V4	battery voltage and current recording
rack and holder	supporting platform
computer	sensor data collection

Table 1: LIST OF EQUIPMENTS

revolution of rotor. Power is supplied by LiPo battery instead of DC power supply because battery has limited discharge rate. And we want to study the dynamics of rotor with the same discharge rate in power source as our actual UAVs.

3 System Identification Method

Both static state analysis and frequency-domain identification methods are utilized for rotor dynamics based on our experiment setup. The static state response can help identify step-response features for interested states, while frequency response can extract richer dynamics information around a trim condition. In this section, main results of these two methods will be presented, and we are mainly concerned with the propeller thrust, torque and angular speed.

3.1 Static state analysis

3.1.1 Stimulus signal

Stimulus signal for static state analysis is shown in lower part of Figure 3, which includes 10 step functions with amplitude increased from 0.1 to 1.0 with step size 0.1. Duration of each step function is 5 seconds therefore total duration is 50 seconds.

3.1.2 Angular speed channel

Result from step signal test indicates the steady-state angular speed when throttle varies from 0.1 to 1.0 with step size 0.1. Table 2 and Figure 3 show the result. As can be observed in

Throttle	Steady-state Angular speed (rad/s)
0.10	228.18
0.20	423.17
0.30	566.85
0.40	689.58
0.50	737.54
0.60	788.02
0.70	832.84
0.80	892.74
0.90	937.35
1.00	941.54

Table 2: RELATION BETWEEN THROTTLE AND STEADY-STATE ANGULAR SPEED

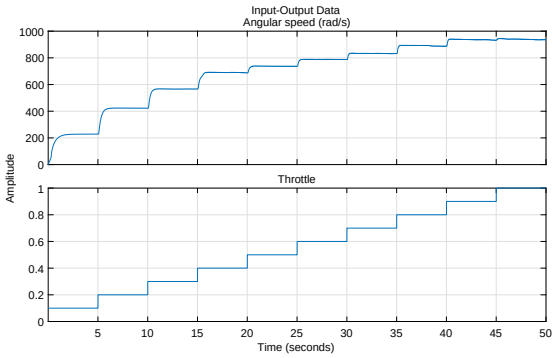

Figure 3: Plot of measured angular speed with corresponding throttle in step signal test

figure and table, angular speed changes proportional to throttle. The relation can be summarized as function:

$$\omega = -1080u^2 + 1952u + 42 (0 \leqslant u \leqslant 1) \qquad (1)$$

where ω is angular speed in rad/s and u is normalized throttle.

3.2 Frequency domain analysis

3.2.1 Stimulus signal

Stimulus signal for frequency domain analysis is selected to be a sinusoidal wave swept from 0.05Hz to 20Hz at throttle equals to 0.6 equilibrium point. The frequency range is selected based on our flight control design as higher frequency exceeds greatly the control bandwidth. However, in order to eliminate effect from battery voltage drop, this chirp signal test has been divided into three experiments:

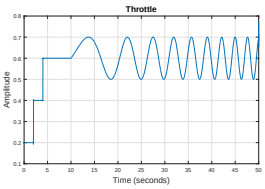

(a) Experiment 1

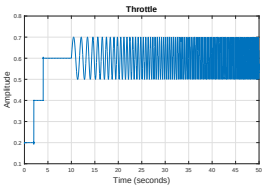

(b) Experiment 2

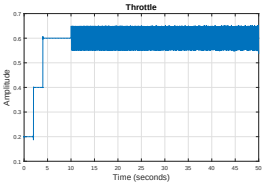

(c) Experiment 3

Figure 4: Chirp stimulus signal

- Experiment 1: Chirp signal swept from 0.05Hz to 0.5Hz, test duration 50s includes 10s warm-up.
- Experiment 2: Chirp signal swept from 0.5Hz to 5Hz, test duration 50s includes 10s warm-up.
- Experiment 3: Chirp signal swept from 5Hz to 20Hz, test duration 50s includes 10s warm-up.

All three chirp signals have been plotted in Figure 4.

3.2.2 Thrust channel

Following figures show the relationship between throttle and thrust in both time domain (Figure 5, Figure 6 and Figure 7) and frequency domain (Figure 8), and this set of data is collected during the chirp signal rotor test. The first 10 seconds warm-up section and mean value will be removed by CIFER during data preprocessing as the response near equilibrium is our interest.

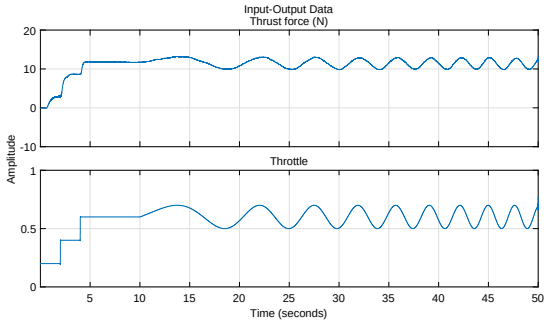

Figure 5: Thrust channel, time domain data of experiment 1

The system in thrust channel has a decreasing gain with frequency. The plot of coherence in Figure 8 indicates the accuracy of frequency estimation. For rotorcraft, recommended

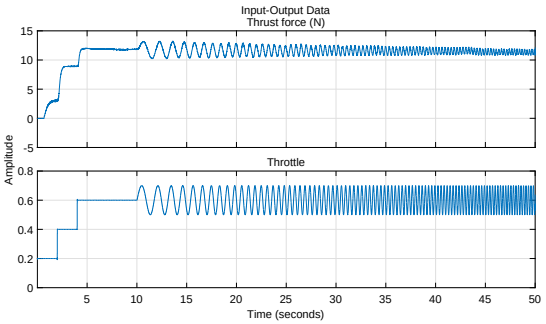

Figure 6: Thrust channel, time domain data of experiment 2

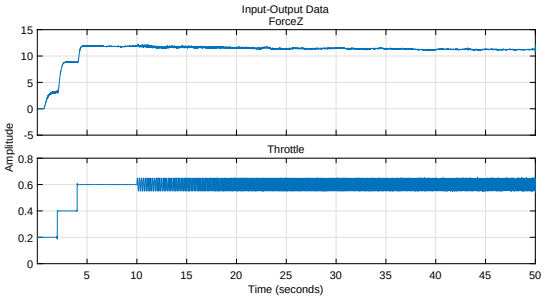

Figure 7: Thrust channel, time domain data of experiment 3

threshold coherence value is 0.6 according to [4]. Therefore, Figure 8 tells that the estimation is credible within the range of frequency up to 30 rad/s. Phase plot suggests that system have a -135 degree phase at 30 rad/s. Hence the system can be approximated by a second order system within confidence range. Then parameter identification is applied and identification result is:

$$\frac{8859}{(s+9.35)(s+61.52)} \tag{2}$$

which DC gain = 15.40, Bandwidth = 9.12 rad/s.

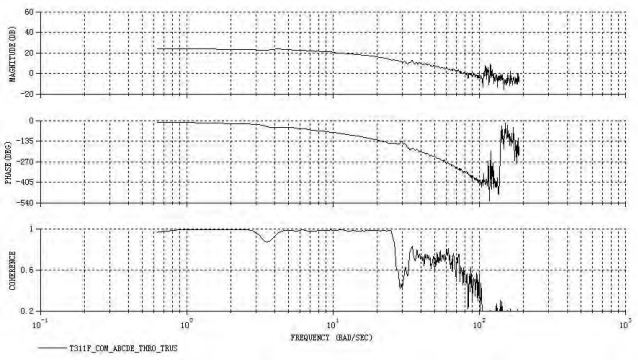

Figure 8: Thrust channel, Bode plot estimated by CIFER

3.2.3 Torque channel and angular speed channel

Similar to thrust channel, the analysis is conducted for torque channel and angular speed channel. Frequency response of torque channel is shown in Figure 9 and estimated transfer function is:

$$23.96\frac{(s+6.02)}{(s+16.94)(s+33.97)} \tag{3}$$

which DC gain = 0.25, Bandwidth = 129.52 rad/s.

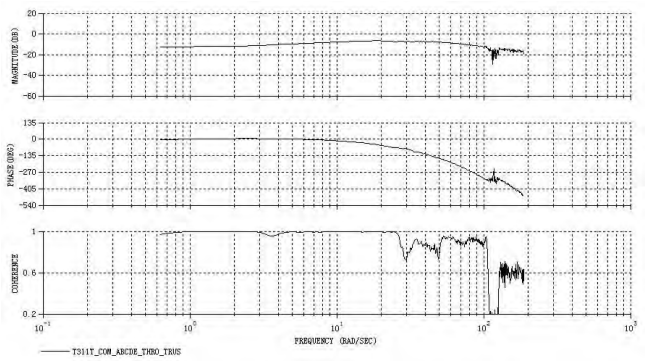

Figure 9: Torque channel, Bode plot estimated by CIFER

Frequency response of angular speed channel is shown in Figure 10 and estimated transfer function is:

$$\frac{225961}{(s+9.39)(s+45.34)} \tag{4}$$

which DC gain = 530, Bandwidth = 9.01 rad/s.

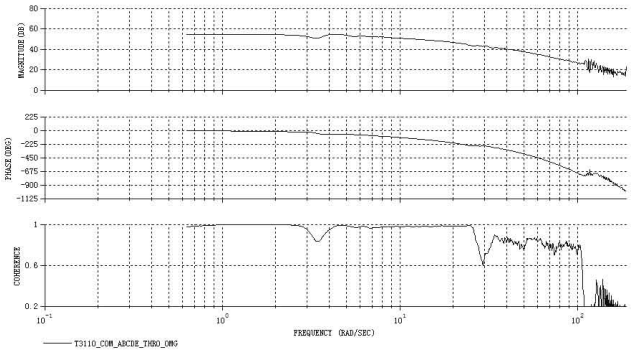

Figure 10: Angular speed channel, Bode plot estimated by CIFER

4 SEMI-EMPIRICAL MODEL OF ROTOR SUBSYSTEM

In previous section, the rotor system is considered as a black-box. The result of identification cannot describe what is happening inside the black-box. In this section, the model of rotor system will be divided into three parts named ESC model, BLDC model and propeller model. Figure 11 shows the block diagram of the the semi-empirical model of rotor subsystem.

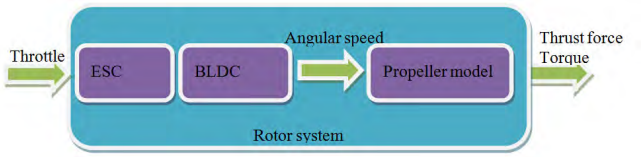

Figure 11: Components of rotor system model

4.1 Propeller model

Propeller model describes the response from angular speed to thrust and torque. According to blade element method, thrust and torque are proportional to the square of angular speed. Therefore, propeller model can be simply constructed as follow:

$$\begin{aligned} F &= K_f\omega^2 + F_{offset} \\ T &= K_t\omega^2 + T_{offset} \end{aligned} \tag{5}$$

where F is thrust force, T is torque, and ω is angular speed in rad/s. K_f ,K_t ,F_{offset} and T_{offset} are unknown coefficients to be identified. This model has been estimated via polynomial fitting based on experimental data obtained, the result is:

$$\begin{aligned} K_f &= 1.814657 \times 10^{-5} \\ F_{offset} &= -4.376713 \times 10^{-1} \\ K_t &= 2.798821 \times 10^{-7} \\ T_{offset} &= -5.700314 \times 10^{-3} \end{aligned} \tag{6}$$

4.2 ESC model and BLDC model

Previous group research suggested a ESC model [5]:

$$\begin{aligned} \omega_d &= throttle^2 K_a + throttle K_b + K_c \\ e_\omega &= \omega_d - \omega \\ u_{eq} &= K_p e_\omega + K_I \int e_\omega dt \end{aligned} \tag{7}$$

where ω_d is desired angular speed and ω is actual angular speed. *throttle* is normalized throttle between 0 and 1. K_a, K_b and K_c are polynomial coefficients describing relationship between throttle and ω. These three parameters have been estimated in section 3 static state analysis. u_{eq} is the equivalent voltage directly input to BLDC, and K_p, K_i are PI gains of control law. The BLDC model is [5]:

$$J_r\dot{\omega} = K_m i - K_r\omega^2 - K_s \tag{8}$$

$$L\frac{di}{dt} = u - Ri - K_e\omega \tag{9}$$

For low inductance BLDC, the above form is further simplified as:

$$J_r\dot{\omega} = -K_s - \frac{K_m K_e}{R}\omega - K_r\omega^2 + \frac{K_m u}{R} \tag{10}$$

where u is the input voltage, J_r is rotor inertia, K_m, K_s and K_e are motor electrical parameters, and *R* is the resistance. The output of ESC u_{eq} is equivalent to u, input of BLDC model.

As only throttle input and angular speed ω are measurable, a nonlinear model of above subsystem is derived as below with an augmented state x_a:

$$\begin{aligned} \dot{\omega} = & \quad -\tfrac{K_s}{J_r} - \tfrac{K_m K_e}{R J_r}\omega - \tfrac{K_r}{J_r}\omega^2 + \tfrac{K_m K_i}{R J_r}x_a + \tfrac{K_p K_m}{R J_r}\omega_d \\ \dot{x_a} = & \quad -\omega + \omega_d \end{aligned} \tag{11}$$

where $K_s, K_m, K_e, K_p, K_i, R$ and J_r are parameters under identification. All parameters are positive.

4.3 Model identification method

Parameter identification is achieved by Matlab function "nlgreyest", which estimates the unknown nonlinear grey-box model parameters based on measured data. The function employs minimization schemes with embedded line searching methods for parameter estimation. Initial value and range of parameters are estimated according to first principle.

4.4 Estimation of parameter range

- Effective motor resistance
  R is effective Motor Resistance. It can be found in data sheet of motor.

- Rotor inertia
  J_r is the moment of inertia of propeller and rotor. This parameter can be estimated by considering them as a thin rod rotating about its middle point. Corresponding formula to calculate J_r is:

$$J_r = \frac{mr^2}{12} \tag{12}$$

  where m is mass of rod and r is radius of the thin rod.

- Equivalent drag coefficient
  $K_r\omega^2$ represents reaction torque from propeller. Therefore, K_r is equivalent to drag coefficient K_f obtained in section 4.1.

- Motor torque constant
  Motor Torque constant K_m can be calculated by applying following formula:

$$K_m = \frac{60}{2\pi K_v} \tag{13}$$

  where K_v is motor velocity constant given in motor data sheet.

- Back EMF constant
  Back EMF constant K_e. In the three phase BLDC motors the relationship is approximately equal to [6]:

$$K_e = \sqrt{\frac{3}{2}} K_m \tag{14}$$

- Static friction torque constant
  K_s is static friction torque constant. It can be measured by torque meter. It usually has much less effect to torque when compared with back EMF and reaction torque of propeller. Hence, it is assumed that this term has 2 order of magnitude smaller than $K_r\omega^2$ term and $\frac{K_m K_e}{R}\omega$ term in equation (10).

- Proportional Gain
  K_p is proportional gain of control law. It can be estimated by using instantaneous angular acceleration while rotor is changing from one trim condition to another. Formula used to estimated K_p is:

$$J_r\dot{\omega} = \frac{K_m}{R} K_p e_\omega \tag{15}$$

  where $\dot{\omega}$ is angular acceleration and e_ω is difference angular speed between two trim conditions.

- Integral Gain
  K_i represents integral gain of control law. It can be estimated by observing the transition from one trim condition to another. equation (7) and equation (10) can be applied to both trim conditions, thus following equations can be obtained:

$$0 = -\frac{K_s}{J_r} - \frac{K_m K_e}{R J_r}\bar{\omega_1} - \frac{K_r}{J_r}\bar{\omega_1}^2 + \frac{K_m K_i}{R J_r}\int e_{\omega 1} dt \tag{16}$$

$$0 = -\frac{K_s}{J_r} - \frac{K_m K_e}{R J_r}\bar{\omega_2} - \frac{K_r}{J_r}\bar{\omega_2}^2 + \frac{K_m K_i}{R J_r}\int e_{\omega 2} dt \tag{17}$$

  $\bar{\omega_1}$ and $\bar{\omega_2}$ are steady-state angular speed for two trim conditions respectively, and both values are measurable. The difference between $\int(e_{\omega 1}dt)$ and $\int(e_{\omega 2}dt)$ can be obtained by integrating e_ω over transition interval between two trim conditions. Therefore, K_i can be estimated by minusing equation (17) with equation (16).

Based on estimated initial values, parameter ranges are defined as shown in Table 3. For parameters calculated from given value in datasheet, range is defined as $\pm 10\%$ of initial value. For parameters calculated from measured data in experiment, range is defined as $\pm 50\%$ of initial value.

4.5 Result and comparison

With aforementioned parameter range and propeller model, Matlab function "nlgreyest" is used to identify the parameters, and the results are shown in Table 4.

Figure 12 and Figure 13 show a comparison between ω from identified semi-empirical model and measured value. In order to verify model fidelity, NRMSE fitness value is used in Matlab, as defined by

$$fit\% = 100\%(1 - \frac{\|p - \bar{p}\|}{\|p - mean(p)\|}) \tag{18}$$

Parameter	Initial value	Range
R	0.014	$\pm 10\%$
J_r	3×10^{-5}	$\pm 50\%$
K_r	2.8×10^{-7}	$\pm 10\%$
K_m	0.01	$\pm 10\%$
K_e	0.012	$\pm 10\%$
K_s	10^{-2}	$\pm 50\%$
K_p	2.6×10^{-4}	$\pm 50\%$
K_i	7×10^{-2}	$\pm 50\%$

Table 3: RANGE OF PARAMETERS

Parameter	Value
R	0.0154
J_r	4.5×10^{-5}
K_r	3.08×10^{-7}
K_m	0.009
K_e	0.0132
K_s	1.5×10^{-2}
K_p	1.3×10^{-4}
K_i	0.069

Table 4: IDENTIFIED PARAMETERS

where p is the validation data collected during experiment and $\bar{p}$ is the output generated by BLDC model. The 75.72% fitness shows that our model prediction fits well with real experiment data.

Another model validation standard is Theil inequality coecient[7] (TIC), which is defined by

$$TIC = \frac{\sqrt{\frac{1}{n}\sum_{i=1}^{n}(\bar{p}-p)^2}}{\sqrt{\frac{1}{n}\sum_{i=1}^{n}(\bar{p})^2} + \sqrt{\frac{1}{n}\sum_{i=1}^{n}(p)^2}} \tag{19}$$

where n is the total sample amount, p is the validation data collected during experiment and $\bar{p}$ is the output generated by BLDC model. TIC is a normalized value between [0, 1], and zero indicates a perfect matching. In practice, the threshold of TIC is commonly set at 0.25 [8]. As for TIC-based validation, results for Experiment 1 and 2 are 0.020 and 0.025 respectively. Both TIC value are much lower than the threshold value 0.25. Therefore, results indicate that identified BLDC model has sufficient accuracy.

After linearized at throttle = 0.6 trim condition, BLDC model is combined with ESC and propeller models, then compared with transfer function obtained through identification approach in section 3. Input is throttle and output is thrust force. Bode plots are shown in Figure 14.

Bode plot of system identified from semi-empirical model has a DC gain equals to 21.8dB and bandwidth 4.95 rad/s. For transfer function identified by CIFER, DC gain is 23.7dB and bandwidth is 9.12 rad/s. The comparison (Figure 14)

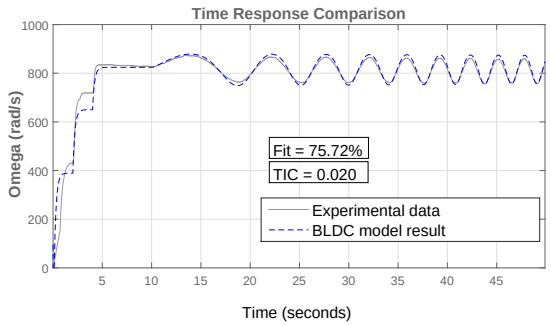

Figure 12: BLDC model result compare with measured angular speed (Experiment 1)

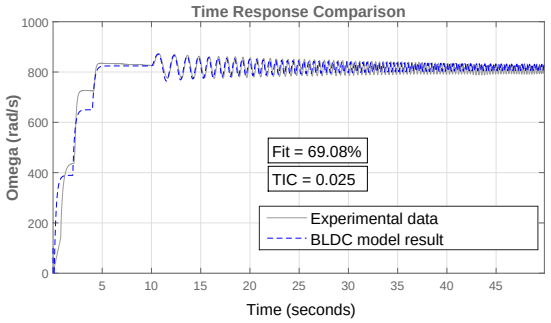

Figure 13: BLDC model result compare with measured angular speed (Experiment 2)

shows that our semi-empirical model can fit well with CIFER identification up to 10 rad/s, and the accuracy implies that our model is capable of predicting rotor dynamics and can be integrated in real-time UAV dynamics and control applications.

5 CONCLUSIONS

To conclude, this paper presents a systematic modeling approach for rotor dynamics integrating brushless DC motor, propeller and ESC. First, static state analysis is done to indicate the behavior under various steady states. Then, frequency responses of dynamics in various channels are successfully generated. Transfer function models are estimated and proven to be reliable for up to 20 rad/s. Finally, a novel semi-empirical model is presented and validated by experimental data. The model is proven to fit well with frequency response results up to 10rad/s and is promising in real-time implementation for UAV dynamics and control.

REFERENCES

[1] B. M. Chen, T. H. Lee, K. Peng and V. Venkataramanan, *Hard Disk Drive Servo Systems*, 2nd ed. New York, NY: Springer, 2006.

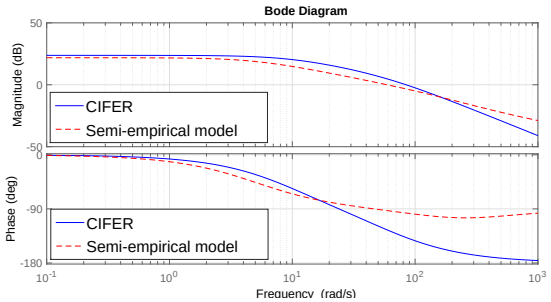

Figure 14: Bode plots of systems estimated by CIFER and by Semi-empirical model. Thrust channel

[2] Ljung L, "Linear Model Identification," in *System identification toolbox*, South Natick, MA:The MathWorks Inc., 1988.

[3] *Comprehensive Identification from Frequency Responses Users Guide*, UCSC, Santa cruz, CA, 2012.

[4] G. Cai, B. M. Chen, T. H. Lee. *Unmanned rotorcraft systems*, New York, NY:Springer Science & Business Media, 2011, pp. 90-94 .

[5] Yijie Ke, "An empirical model to rotor dynamics with brushless DC motor," Internal report in NUS unmanned system research group.

[6] *General motor terminology*, The Motor & Motion Association, S. Dartmouth, MA, 2015.

[7] M. B. Tischler, R. K. Remple , *Aircraft and rotorcraft system identification: Engineering methods with flight test examples*, VA:American Institute of Aeronautics and Astronautics, 2006.

[8] G. Cai, T. Taha, J.Dias amd L. Seneviratne, "A framework of frequency-domain flight dynamics modeling for multi-rotor aerial vehicles,". *Journal of Aerospace Engineering*, May. 2016.